Hydrodynamics in the Blade Region of a Self-Aspirating Disk Impeller

J. Stelmach[†] and R. Musoski

Lodz University of Technology, Faculty of Process and Environmental Engineering Wolczanska 213, 90-924 Lodz, Poland

†*Corresponding Author Email: jacek.stelmach@p.lodz.pl*

ABSTRACT

In studies of self-aspirating impellers found that gas bubbles are not broken down by the impeller blades. Break-up of bubbles is caused by the eddies generated by the blades. Therefore, to describe how the liquid flow near the blades is an important research issue for this type of impellers. Using the PIV method average velocity fields in the axial-radial plane between baffles in the stirred tank were defined for seven different positions of blades of a self-aspirating disk impeller in relation to that plane. It was found that in the small space in blade vicinity, big changes in fluid circulation were observed depending on the position of the blade relative to the baffle. In front of blade the liquid from bottom and from over impeller is directed radially towards the wall of tank and the average axial velocity is zero. Behind the blade the cavern (cavity) is formed, understood as a space of reduced pressure. Underpressure causes suction effect which directs the liquid inside the cavern. In just a few millimeters from the blade tip average axial and radial velocities are equal to zero. In this region the tangential component of velocity is dominant.

Keywords: Cavern, mixing; PIV; Self-aspirating disk impeller; Velocity distribution; Velocity pulsation.

NOMENCLATURE

D	impeller diameter	Re	Reynolds number
g	acceleration due to gravity	U_{tip}	tangential velocity of the blade tip
H	height	U	velocity
Fr'	modified Froude number	U^*	dimensionless velocity
h	height		
h	distance of the impeller from the tank bottom	u'^*	dimensionless velocity pulsation in RMS sense
N	rotational frequency of the impeller	η	dynamic viscosity coefficient
R	radius	ρ	density

1. INTRODUCTION

Self-aspirating (gas-inducing) impellers disperse gas in a liquid without additional installations of compressed gas (Saravanan *et al*., 1994, Saravanan and Joshi, 1995, Forrester *et al*., 1997, Patwardhan and Joshi, 1999, Deshmukh *et al*., 2006,). The mass transfer rate is determined by hydrodynamic conditions (Poncin *et al*., 2002). The most important is the region near the impeller blades (Kuncewicz and Stelmach, 2012). Self-aspirating impellers work effectively when modified Froude number *Fr'* is much larger than the critical value (Forrester *et al*., 1998, Evans *et al*., 1992, Ju *et al*., 2009). For the

description of the phenomena occurring during gas dispersing it is necessary to know the liquid flow in the impeller region. However, the study of the two-phase gas-liquid system is a difficult task. Therefore, the first step in such studies may be a description of hydrodynamics for single-phase system.

Determination of liquid circulation in a stirred tank and its mean velocities is an issue with a long history. For laminar flow the distribution of liquid velocity in the tank can be identified with high accuracy by mathematical modeling (Kuncewicz and Pietrzykowski, 2006, Kuncewicz *et al*., 2013). A much more difficult problem is to obtain a similar

distribution for turbulent mixing. But even in this field steady progress is observed. In computational fluid dynamics (CFD) are used models with varying levels of complexity (Joshi *et al.*, 2011a, Joshi *et al.*, 2011b, Gillissen and Van den Akker, 2012). There is also commercial software (eg. ANSYS, Comsol Multiphysics) that calculates distributions of velocity, pressure and energy dissipation rate in stirred tank. Still, the calculation results are verified by comparison with experimental data.

Initially, on the basis of measurements in selected points of a tank (Pitot tube, hot-wire anemometer, *LDA*) the experimental profiles of velocity components were determined. Technological development brought about new research methods. One of them is the Particle Image Velocimetry (*PIV*) which is used to determine many local velocities within a large measurement area at the same time. In this way a map of velocity vectors showing the fluid flow direction and velocity is obtained. A big advantage of this method is the ability to synchronize the measurement with the impeller movement. This means that measurements can be made for a fixed position of the blade relative to the plane of measurement. This is important because studies show a significant difference in the measured velocities in the cases of fixed and random positions of the blade relative to the plane of measurement (Heim and Stelmach, 2011).

A large part of the information about velocity distributions into stirred vessel refers to two types of impellers: Rushton turbine and pitch blade turbine (e.g. Wu and Patterson, 1989, Kresta and Wood, 1993, La Fontaine and Shepherd, 1996, Myers *et al.*, 1997, Lee and Yianneskis, 1998, Sharp and Adrian, 2001, Escudié and Liné, 2003, Aubin *et al.*, 2004). This is due to the wide dissemination of these impellers in the industry. For self-aspirating impellers is much less information in literature (Murthy *et al.*, 2007, Murthy *et al.*, 2008). In our study by LDA method the profiles of average velocities and RMS were determined in planes: symmetrically between baffles and 2.5° behind baffle (Stelmach *et al.*, 2002, Rzyski and Stelmach, 2002). The contour plots of tangential velocity was also obtained by PIV method (Stelmach, 2014).

The aim of the study is to examine liquid hydrodynamics in the vicinity of the blade of a self-aspirating disk impeller operating without gas dispersion at rotational frequency slightly higher than the critical rotational frequency.

An exact description of liquid circulation and pulsations in these conditions will allow us to extend knowledge on the mode of operation of the self-aspirating impellers and will be an introduction to a model of their functioning. During the impeller operations, at the beginning of self-aspiration the number of gas bubbles is small and practically they do not disturb the movement of liquid. However, light is reflected from the interface which causes that bubble images are recorded by the camera of the *PIV* system. This leads to falsification of the measurement results. To solve this problem

measurements should be carried out using two cameras and fluorescent markers. Measurements in a single-phase system are more precise and easier to perform. So, it was decided to study and describe the liquid flow behind the blade of the self-aspirating impeller without the gas phase. As this is an initial stage of research, we restricted the measurements to axial and radial components of velocity. In the future, to obtain a full image of hydrodynamic phenomena it will be necessary to supplement the results with a peripheral velocity component.

2. EXPERIMENTAL

Experiments were carried out in a flat-bottomed glass tank of diameter $T = 292$ mm equipped with four baffles of width $B = 0.1 \cdot T$. The self-aspirating disk impeller of diameter $D = 125$ mm was placed at height $h = 78$ mm above the tank bottom. The tank was filled with distilled water ($t = 20°C$) to the height $H = 0.3$ m. Glass tracer particles of mean diameter 10 μm were added to water. To reduce optical distortions, a cylindrical tank was placed in a rectangular tank and the space between the walls of the tanks was filled with water. Velocity measurements were made for rotational frequency of the impeller $N = 360$ min^{-1} in the plane defined by the axis of rotation of the impeller and the bisector of the angle between the baffles (Fig. 1). In the measurement conditions the Reynolds number was $Re = 93580$ and the modified Froude number $Fr' = 0.258$. The impeller was operating without gas dispersion (the inlet in the shaft was stopped).

The measurements were made using a *LaVision* PIV measuring system with a double-pulse laser with maximum power of 135 mW and an *ImagePro* camera with 2048 px × 2048 px resolution equipped with a *Nikkor* 1.8/50 lens. The aperture of the lens was stopped down to the value ensuring a maximum resolution (the f-number was 5.6). The measurement area was approximately 60 mm × 60 mm. Laser pulses were initiated by an external trigger. The thickness of the light knife was 1 mm. Due to the importance of the area near the impeller blade where during a normal operation gas bubbles are subjected directly to eddies formed behind the blade, measurements were made for seven angular positions of the blade relative to the measurement plane at distances -15°, -10°, -5°, 0°, 5°, 10° and 15° in relation to the light knife (Fig. 1). For each angular position of the blade 200 double photographs were taken to velocity averaging. Time interval between the pulses was $\Delta t = 415$ μs. This value was calculated on the assumptions: 1 - radial and axial velocities are less than 20% of tip blade velocity, 2 – pixel shift (displacement of tracer particles at the photographs) 10 pixels. The limit value for the first assumption was defined on the basis of previous measurements by LDA method (Stelmach *et al.*, 2002).

Data processing was performed using the *DaVis* 7.2 program. Two-pass data processing was used with the final size of analyzed area being 32 px × 32 px (i.e. about 0.95 mm × 0.95 mm) without overlaying.
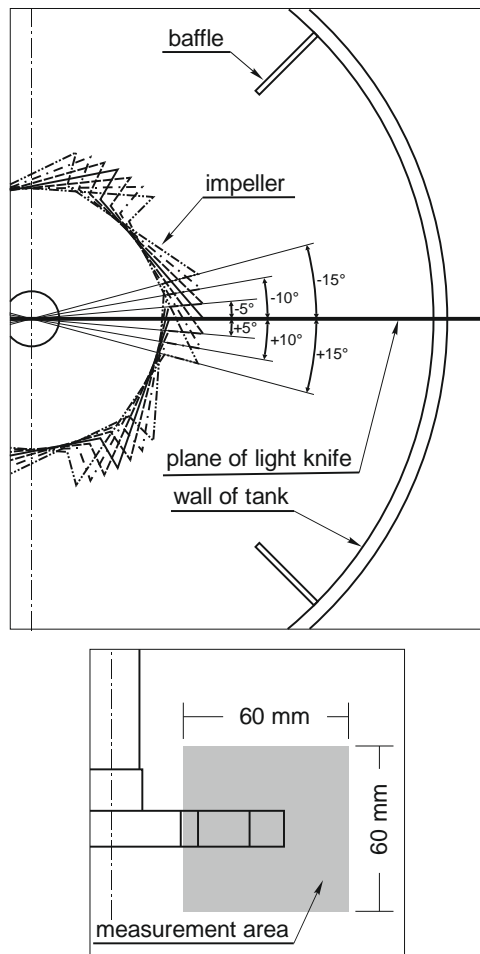
Fig. 1. Schematic diagram of the measurement system.

3. RESULTS AND DISCUSSION

The authors are convinced that the use of an external trigger of laser pulses synchronized with the position of the blade in relation to the light knife plane can eliminate the effect of a component of periodic velocity pulsation on results obtained (Wu and Patterson, 1989, Kresta and Wood, 1993). In the case of an impeller tested earlier by the *LDA* method it was confirmed that such a component occurred, e.g. as peaks in the energy spectrum for the frequency equal to the blade passage frequency (Stelmach *et al.*, 2003a, Stelmach *et al.*, 2003b, Kurasiński *et al.*, 2004).

Literature data (Baldi and Yianneskis, 2003) and our own studies (Heim and Stelmach, 2011) show that in the PIV method it is enough to average 100 instantaneous velocities in order to obtain small errors. In this study the number of measurements has been doubled.

For the side position of the camera, the *PIV* system determines velocity components in the horizontal (radial component) and vertical direction (axial component) in the centers of squares into which the entire image field is divided (interrogation area). This makes it possible to calculate resultant velocity in the *r* - *z* plane and the angle between the resultant

velocity vector and the level. To facilitate the analysis of velocity distributions and flow direction, it was decided to present results in the form of contour plots and distributions of velocity vectors in the *r* - *z* plane.

The paper is limited to discuss the results for rotational frequency $N = 360$ min^{-1}. However, the measurements performed for $N = 360$ min^{-1} and $N = 420$ min^{-1} shows that dimensionless velocity distributions for both rotational frequency are very similar. Comparison of the both distributions is shown in Fig. 2. The similarity of distributions allows you to extrapolate the results in specified range of impeller rotational frequency.
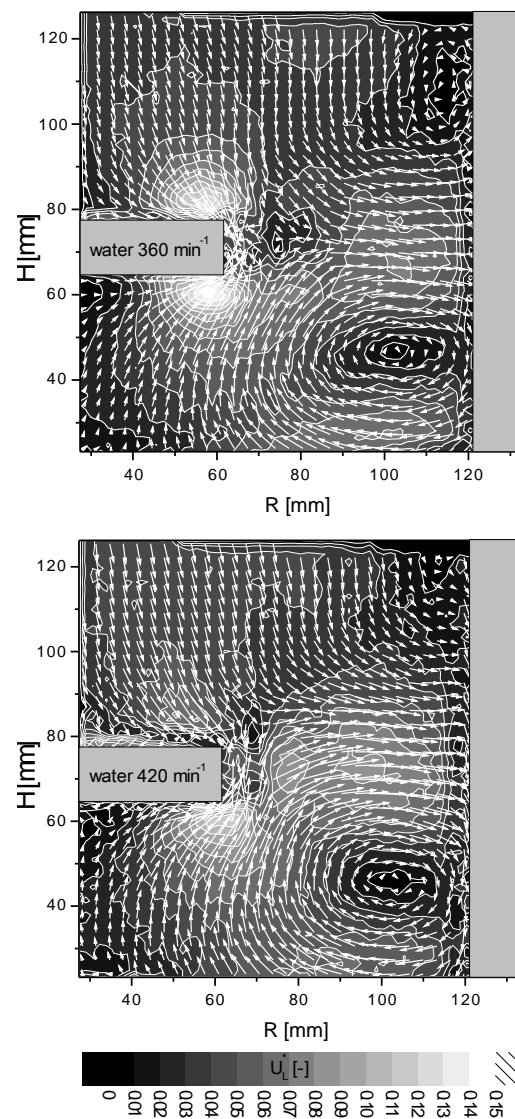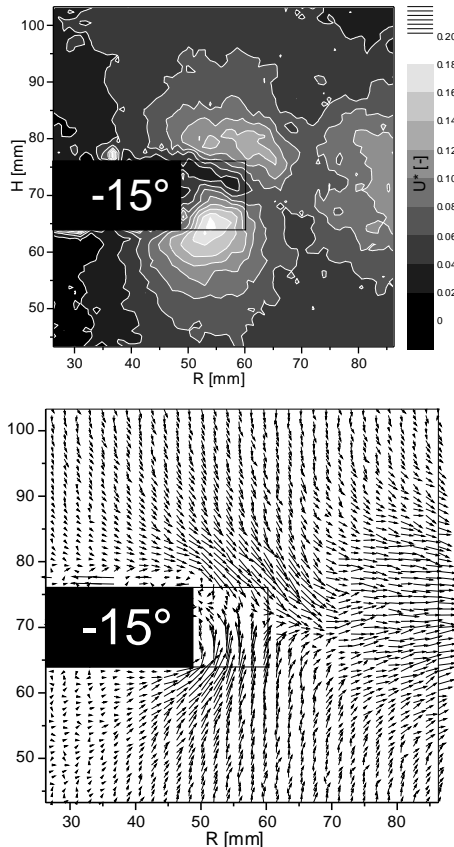

Fig. 2. Comparison of dimensionless velocity distributions for $N = 360$ and 420 min^{-1}.

3.1 Blade 15° Behind the Light Knife

Figure 3 shows a contour plot of liquid dimensionless velocities (i.e. after dividing by the velocity of the blade tip U_{tip}) and vector plot which shows the direction of flow.

**Fig. 3. Contour plot of the liquid dimensionless velocities for blade 15° behind the light knife.**

In the middle height of the impeller about 5 mm from the blade tip two liquid streams merge. One flows from upwards and the other one is generated by liquid circulation below the impeller (Kurasiński and Kuncewicz, 2009). The highest velocities are observed in the corners of the blades. In the combined stream flowing radially from the impeller to the wall average velocities do not exceed 15% of the blade tip velocity.

At the impeller level a flow is radial like for Rushton turbine. More detailed information about liquid flow can be obtained after the separation of velocity components. Figs. 4 and 5 show the contour plots (maps) of axial and radial velocity.

Since the analysis of velocity maps is difficult because of the very large amount of information also the velocity profiles were showed. Axial flow is symmetric relative to the center height of the impeller. At this level the axial velocity is equal to zero. While the radial velocity increases towards the tank wall and all profiles have similar waveforms.

Figure 6 shows a contour plot of dimensionless averaged velocity pulsations (in RMS sense) for the two measured components. The highest velocity pulsations occur at the impeller height starting from the base of the blade up to several millimeters from its tip. This area covers also the place where the streams of circulating liquid merge. In this area root mean-square velocity pulsations reach 30% of the blade tip velocity and exceed average velocities. Outside this area the distribution of pulsations is
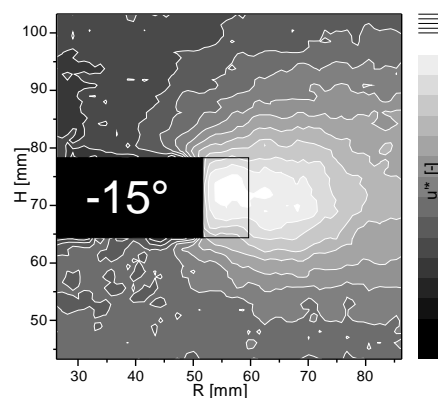
quite uniform. The smallest pulsations occur above the impeller near the shaft.
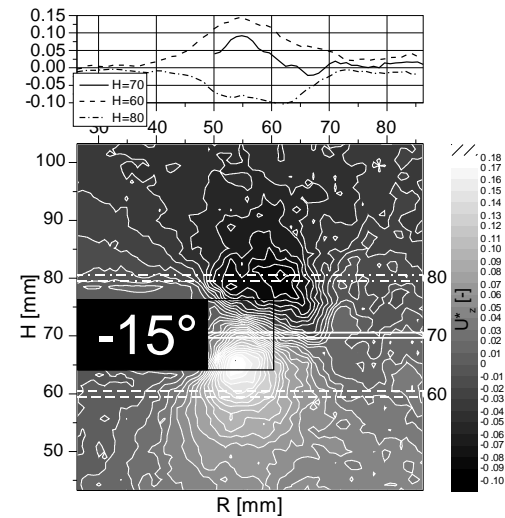
Fig. 4. Dimensionless axial velocities for blade 15° behind the light knife.
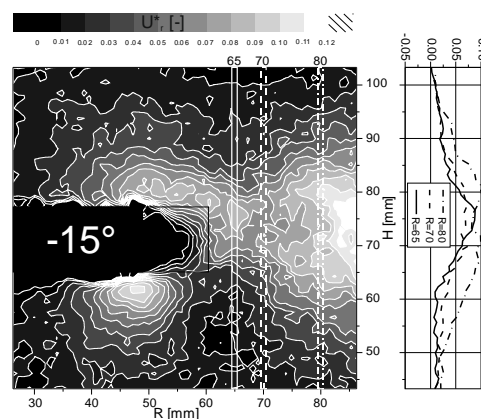
Fig. 5. Dimensionless radial velocities for blade 15° behind the light knife.


**Fig. 6. Dimensionless root mean-square velocity pulsations for blade 15° behind the light knife**.

The energy dissipation rate ε is associated with the RMS. Therefore, the distribution of root mean-square velocity pulsations can be also treats as the quality distribution of ε.

3.2 Blade 10° Behind the Light Knife

Rotation of the impeller by 5° hardly changes liquid circulation in the analyzed area. Still at the height of the impeller several millimeters from the blade tip one can observe merging of streams from above and below the impeller (Fig. 7, 8 & 9). However, closer examination shows that velocity distributions change.
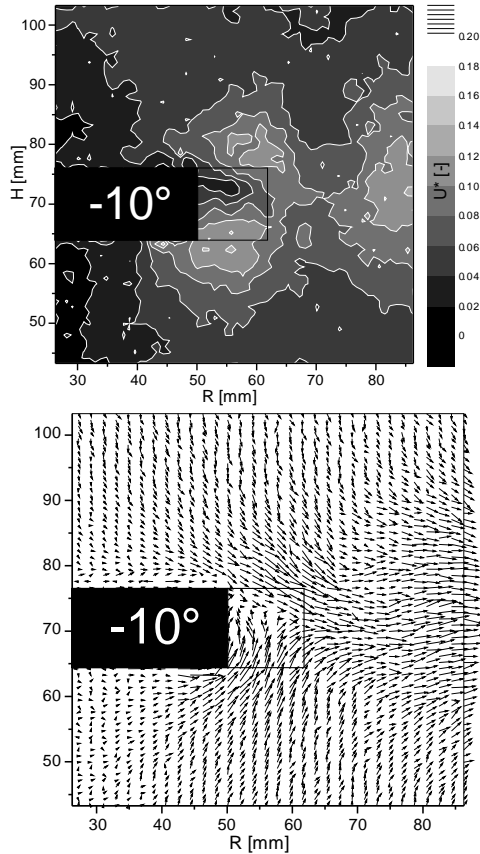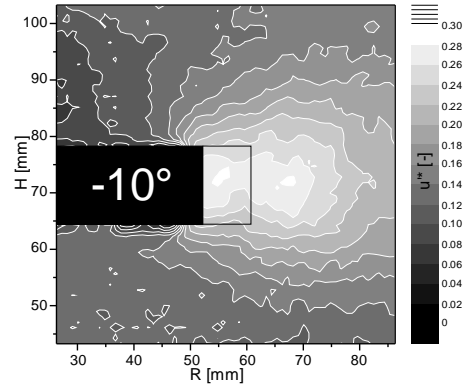

Fig. 7. Contour plot of the liquid dimensionless velocities for blade 10° behind the light knife.
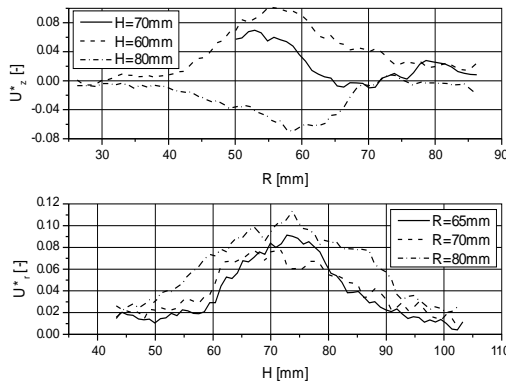
Fig. 8. Axial and radial velocity profiles for blade 10° behind the light knife.

Axial velocity profiles for $H = 60$ mm and $H = 80$ mm are still symmetrical, but the absolute maximum values are lower than for the position -15°. The maximum values of radial velocities also increased. Radial velocities have similar values in all

studied cross-sections of the tank. Their maximum values are slightly higher than for -15°.
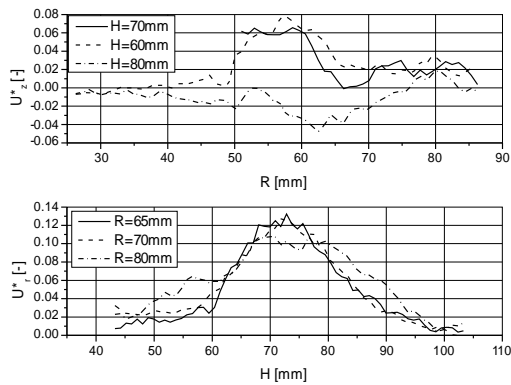

Fig. 9. Dimensionless root mean-square velocity pulsations for blade 10° behind the light knife.

3.3 Blade 5° Behind the Light Knife

Figure 10 shows distributions of average dimensionless velocities for the position of blade 5° in front of the light knife. The nature of liquid circulation compared to the previous position has been slightly changed. There is a shift of maximum velocities from the blade corners to the point in the middle of the height of the impeller about 10 mm from the blade tip.
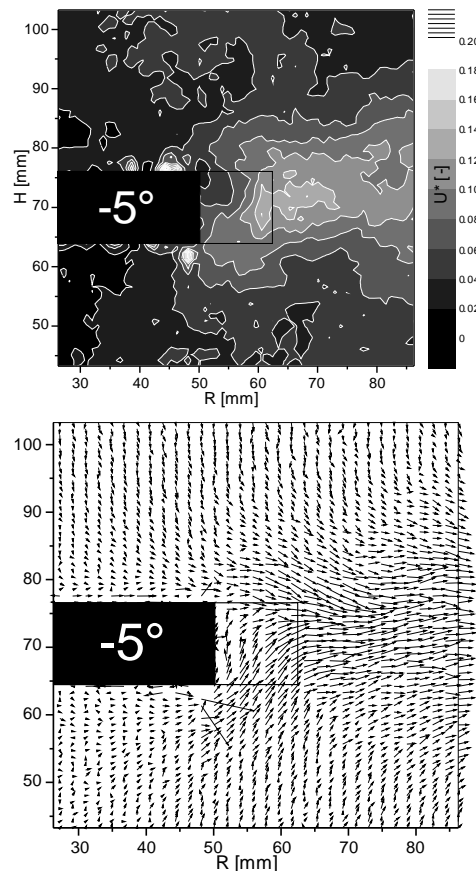

Fig. 10. Contour plot of the liquid dimensionless velocities for blade 5° behind the light knife.

Fig. 11. Axial and radial velocity profiles for blade 5° behind the light knife.

Axial velocity profiles have not changed in comparison to the previous position. Radial velocity profiles are nearly identical and maximum values are greater than for positions -10° and -15°.

The highest values of velocity pulsations decreased by about 15% compared to the previous blade position (Fig. 12) which means that turbulence at this distance from the impeller blade had no time yet to fully develop.
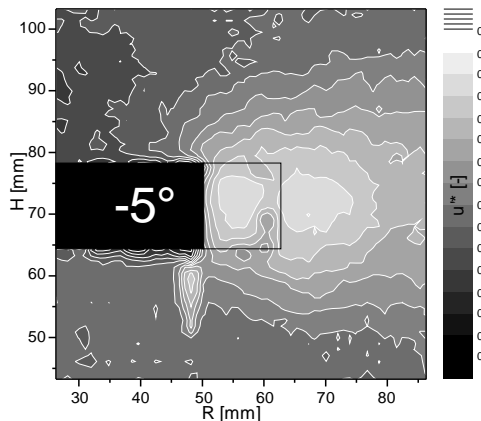

Fig. 12. Dimensionless root mean-square velocity pulsations for blade 5° behind the light knife.
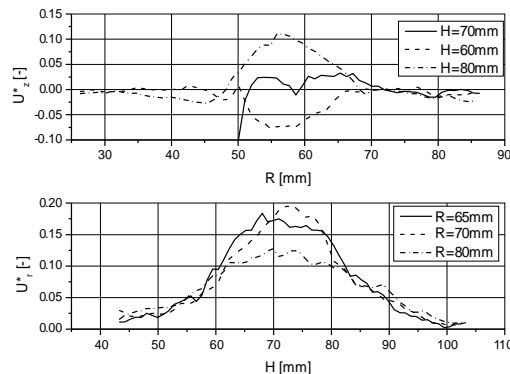
3.4 Blade in the Light Knife Plane (0°)

In the plane passing through the impeller blade the flow of liquid changes substantially (Fig. 13).

The rotating blade forces the liquid simultaneously in three directions: upward, downward and towards the wall. Streams flowing up and down meet the streams of liquid circulating above and below the impeller and are directed radially towards the wall. Similarly, as for the position of blade 5° in front of the light knife the maximum liquid velocity occurs in the middle of the height of the impeller about 5 mm from the blade tip. At this point the velocity of radially flowing liquid stream exceeds even 20% of the blade tip velocity. It is easy to observe a significant change in the nature of distribution of resultant velocities in comparison with previous blade positions (Fig. 3, 7 and 10).
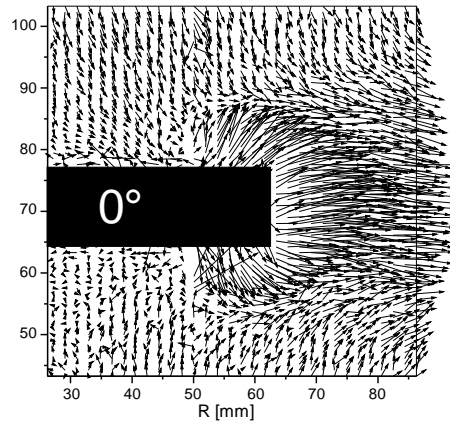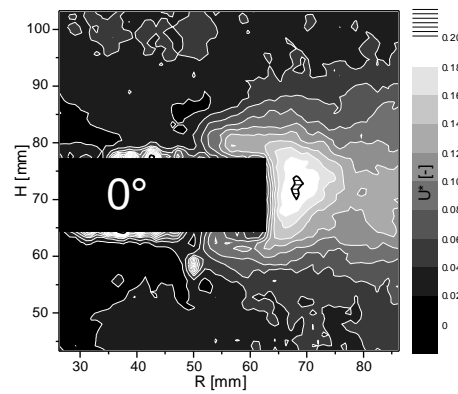
Fig. 13. Contour plot of the liquid dimensionless velocities for blade in the light knife plane.

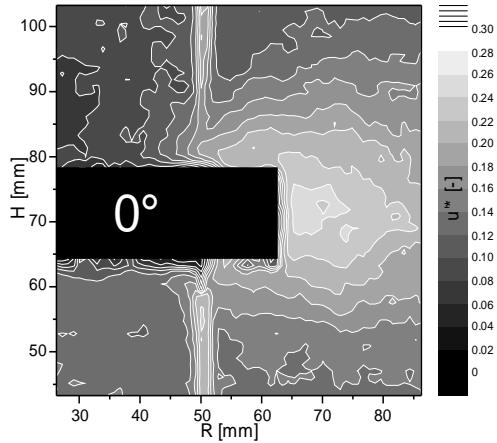**Fig. 14. Axial and radial velocity profiles for blade in the light knife plane.**

In the case of axial velocity profiles the inversion is observed in comparison to the previous positions of the blade – over impeller liquid flows up. The maximum value of the radial velocities are further increased as compared to the position -5° and reach 20% of blade tip velocity U_{tip}.

For liquid in the plane of the impeller blade the maximum velocity pulsations decreased but their positions on the analyzed area did not change (Fig. 15). This means that the strong orientation of liquid flow from the blade to the wall of the tank suppresses velocity pulsations.
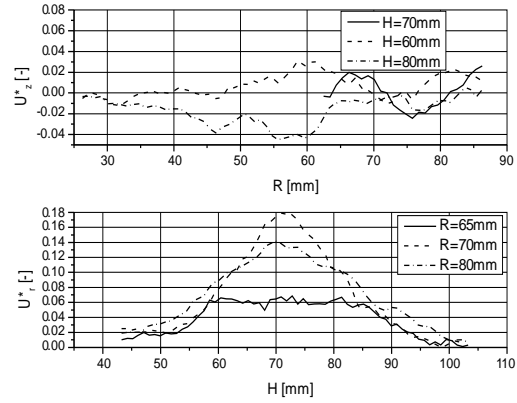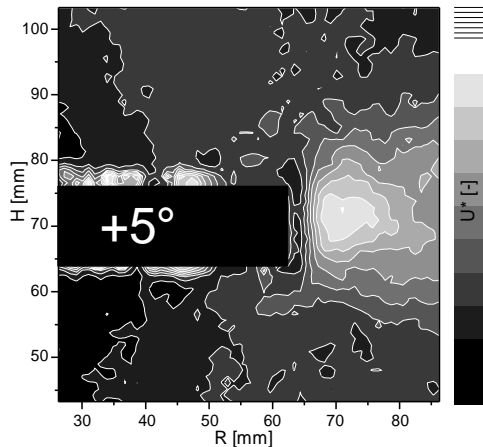
3.5 Blade 5° in Front of the Light Knife

After rotating the blade by further 5° liquid circulation in the measurement area is a mirror image

relative to the position of blade 5° in front of the light knife. However, for the current position there is a clearly visible area of high velocities in the middle of the blade height and tank radius R = 72 mm (Fig. 16). For blade position -5° such an area did not appear.
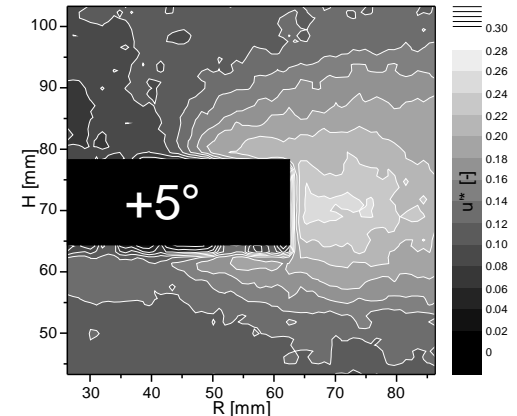

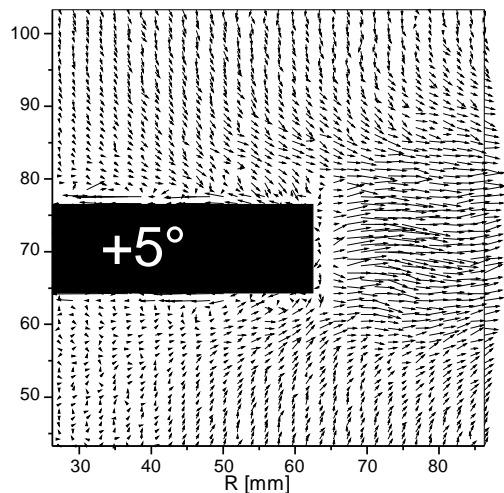**Fig. 15. Dimensionless root mean-square velocity pulsations for the light knife plane.**

Fig. 17. Axial and radial velocity profiles for blade 5° in front of the light knife.

Axial velocities are lower than in the case while the blade is located behind the light knife. Again, the liquid from over the impeller flows down. Radial velocities decrease, especially near the blade tip.

The contour plot of velocity pulsation distribution is similar to the plot for position -5° (Fig. 18). The maximum root mean-square velocity pulsations did not exceed 25% of the blade tip velocities.


**Fig. 18. Dimensionless root mean-square velocity pulsations for blade 5° in front of the light knife.**

3.6 Blade 10° in Front of the Light Knife

Upon shifting of the blade by further 5° a change of flow is observed near the blade corners (Fig. 19). The liquid flowing from above and below the impeller does not pass towards the tank wall but flows at a relatively high velocity (above 15% U_{tip}) behind the blade. This suggests that the blade products a cavity, i.e. the space with reduced pressure giving the effect of gas 'aspiration'. During normal operation of the impeller (with opened inlet on the shaft) gas bubbles separated from the interface of the gas bubble inside the impeller are aspirated into the cavity. The aspirating effect of the cavity causes that in the space from the blade tip to $R \approx 72$ mm radial and axial velocities are equal nearly to zero (in this space there is virtually only peripheral velocity component). For larger radii the liquid flows radially towards the wall, as for the previously discussed blade positions.

Fig. 16. Contour plot of dimensionless liquid velocities for blade 5° in front of the light knife.
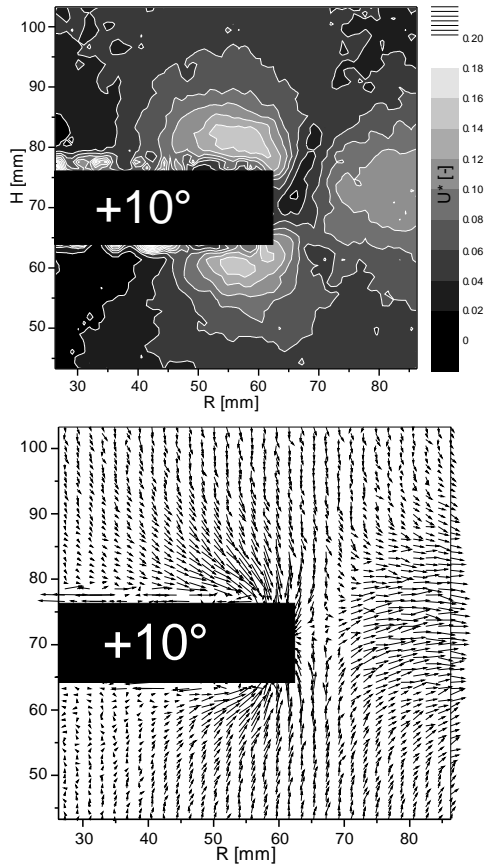
Fig. 19. Contour plot of dimensionless liquid velocities for blade 10° in front of the light knife.
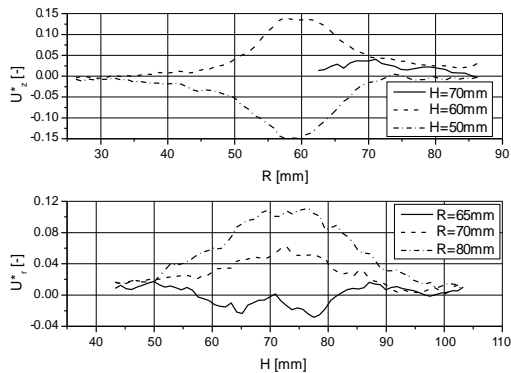

Fig. 20. Axial and radial velocity profiles for blade 10° in front of the light knife.

For this position of blade the increasing of axial velocities is observed relative to the previous position. Maximum values ale larger than for position -10°. At short distance from the blade radial velocities are almost equal to zero. These velocities increase toward the wall of tank. However, they are less than for the previous position of the blade.

In relation to the previous blade position the biggest velocity pulsations increased (to about 30% U_{tip}) and the pulsation distribution was very similar to the distribution for position -10° (Fig. 21). An increase of the maximum values of energy dissipation rate was also observed. However, the area of this increase is small and its importance in the process of gas

bubble disruption during gas dispersion is also small (at a small number of bubbles it is little probable that a bubble can appear in this area).
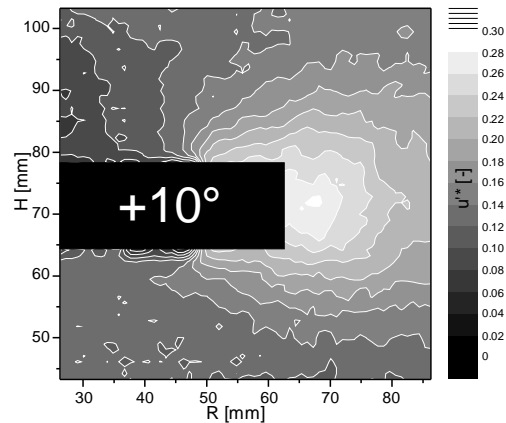
Fig. 21. Dimensionless root mean-square velocity pulsations for blade 10° in front of the light knife.

3.7 Blade 15° in Front of the Light Knife

In this blade position the circulation of liquid does not differ from that observed for position +10°. The liquid flows at a high rate into the cavity behind the blade (Fig. 22).

Axial and radial velocity profiles are nearly identical to the blade position +10°.
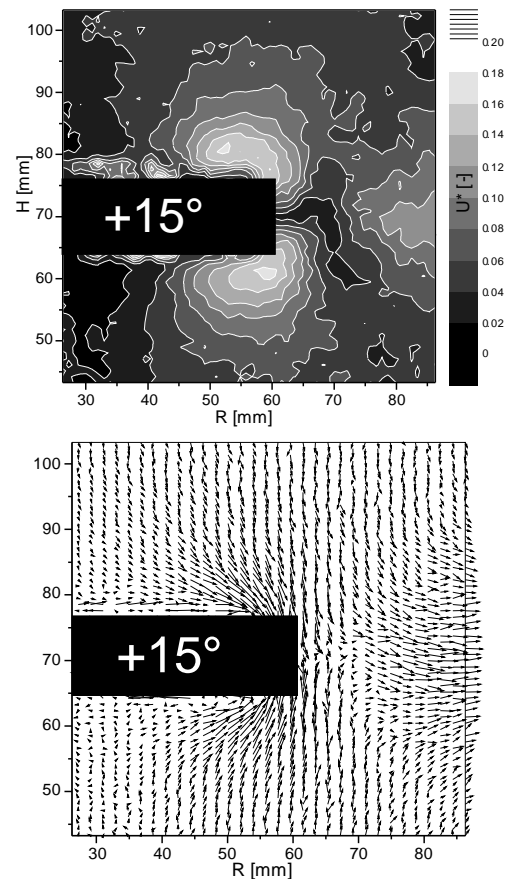
Fig. 22. Contour plot of dimensionless liquid velocities for blade 15° in front of the light knife.

Fig. 23. Axial and radial velocity profiles for blade 15° in front of the light knife.

The distribution of velocity pulsations corresponds to the distribution for position -15° (Fig 24).

3.8 Tangential Velocity

During recent studies (Stelmach, 2014) the dimensionless tangential velocities at the impeller level were received (for the same conditions $N = 360$ min^{-1}). The results are shown in Fig. 25. The tangential velocity distribution is almost symmetric with respect to the plane lying at mid-height of the impeller.
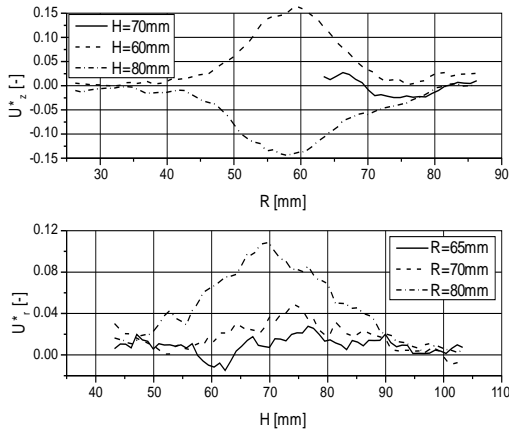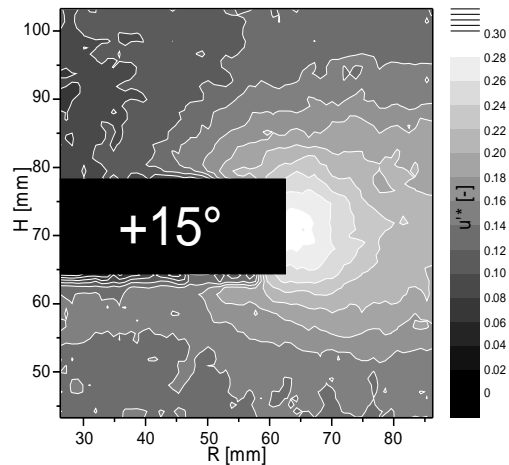

Fig. 24. Dimensionless root mean-square velocity pulsations for blade 15° in front of the light knife.

Behind the blade there is a small area where the liquid velocities exceeds the velocity of the blade tip (U_{tip}). There is this pressure causes a suction effect which was observed for radial and axial component for blade positions +10° and +15° (Figs. 19 & 22). Already 2 mm above and below the impeller maximum velocities reach only several percent of the tip blade velocity.
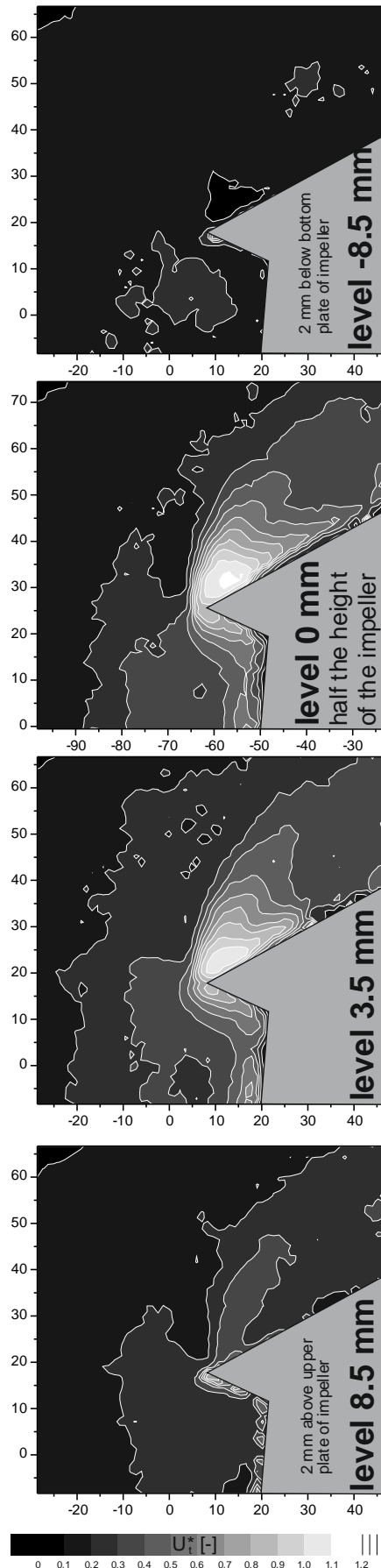
Fig. 25. Contour plots of dimensionless tangential velocities at the impeller level.
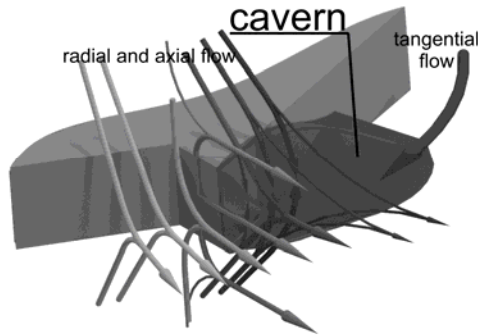
Fig. 26. The shape of the cavern behind blade and directions of liquid flow.
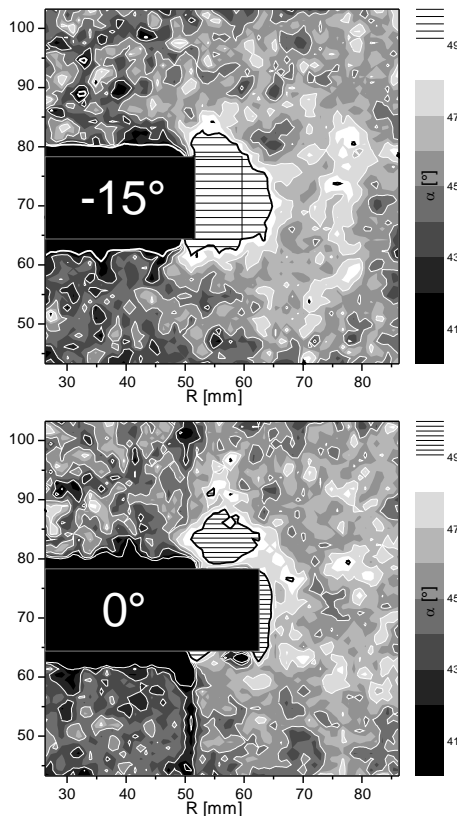
Fig. 27. Contour plots of angles between the resultant velocity pulsation and the level.

3.9 Flow around the Impeller

The biggest changes in liquid velocity during rotations of the impeller can be observed inside a ring of inner radius 50 mm, external radius 75 mm and bases distant by 10 mm from the horizontal surfaces of the impeller. In front of the blade the streams of liquid circulating in eddies above and below the impeller merge together at the height of the impeller and flow towards the tank wall (Fig. 26). Behind the blade of self-aspirating disk impeller the cavern is created. It can be understood as an area of low pressure (reduced pressure area). Part of liquid streams are directed to the cavern. The flow to cavern is so strong that at a distance of about 5 mm from the blade tip the average radial and axial velocities are close to zero. Beyond this space changes of velocity in the measurement area are minimal and do not depend on the position of blade against the light knife.

The shape of the cavern can be determine on the basis of measurements of all velocity components. It is shown in Fig. 26. Inside the cavern tangential velocity exceeds the velocity of blade tip U_{tip}.

3.10 Isotropy of Turbulence

Due to the future use of root mean-square velocity pulsations to energy dissipation rate calculating, the isotropy of turbulence for axial and radial components was investigated. In the case of isotropic turbulence the velocity pulsations in both directions should be the same. This means that the angle between the line of resultant velocity pulsation and the horizontal line (level) should be equal to 45°. Fig. 27 shows a contour plots of distribution of these angles for blade positions -15° and 0°. Analysis of this Figure leads to the conclusion that outside the blade region there is a nearly isotropic turbulence (for the analyzed components).

Table 1 Correlation coefficients R_c

position	R_c	
	all data	outside the impeller
-15°	0.705	0.956
-10°	0.662	0.950
-5°	0.595	0.944
0°	0.721	0.943
+5°	0.595	0.944
+10°	0.673	0.944
+15	0.649	0.946

The correlation coefficient between pulsation components of axial and radial velocities should have a value close to unity for isotropic turbulence. The *CORREL* function of *MS Excel* was used to calculate the correlation coefficient between two data sets. The results for all data and data from outside the impeller region defined as $R < 70$ mm and 60 mm $< H < 80$ mm was shown in Table 1.

The data of Table 1 confirm that outside the impeller region the turbulence is isotropic. This confirms the results of previous investigations with using *LDA* method (Rzyski and Stelmach, 2002).

4. CONCLUSIONS

PIV method provides large amounts of information about velocity field. However, the investigation of the similarity of velocity fields is a difficult issue. Helpful may by statistical methods.

Self-aspirating disk impeller generate a tangential and radial flow of liquid, as a Rushton turbine. The highest velocities are observed within a short distance (a few millimeters) from the impeller. At the impeller level the radial velocities have greatest

values, which, however do not exceed 20% of U_{tip}. The maximum values of axis velocities reach 15% of U_{tip}. The values of all velocity components quickly decrease when moving away from the impeller.

The liquid flow behind and in front of blade is different. Behind the blade of self-aspirating disk impeller the cavern is formed. Inside the cavern liquid velocities greater then velocity of blade tip are observed.

For the tested range of blade positions there is a symmetry of velocity pulsation distributions relative to the plane determined by the tank axis and angle bisector between the baffles. The highest pulsations were observed for blade position 15° in front of and behind the plane determined by the tank axis and bisector of the angle between the baffles. High values of the velocity pulsations occur also in the area of small average velocities.

Apart from the small space next to the blades, the isotropy of turbulence of the stirred liquid is observed for the components of radial and axial velocities.

ACKNOWLEDGEMENTS

REFERENCES

Aubin, J., N. Le Sauze, J. Bertrand, D. F. Fletcher and C. Xuereb (2004). PIV measurements of flow in an erated tank stirred by a down- and up-pumping axial flow impeller, *Experimental Thermal and Fluid Science* 28, 447-456.

Baldi S. and M.Yianneskis (2003). On the direct measurement of turbulence energy dissipation in stirred vessels with PIV, *Industrial Engineering and Chemical Research* 42, 7006-7016.

Deshmukh. N. A., S. S. Patil and J. B. Joshi (2006). Gas induction characteristics of hollow self-inducing impeller, *Chemical Engineering Research and Design* 84(A2), 124-132.

Escudié, R. and A. Liné (2003). Experimental analysis of hydrodynamics in a radially agitated tank, *IAIChE Journal* 49, 585-603.

Evans, G. M., C. D. Rielly, J. F. Davidson and K. J. Carpenter (1992). Hydrodynamic characteristics of a gas-inducing impeller, *Fluid Mechanics of Mixing* 10, 153-161.

Forrester, S. E., C. D. Rielly and K. J. Carpenter (1998). Gas-inducing impeller design and performance characteristics, *Chemical Engineering Science* 55, 603-615.

Gillissen, J. J. J. and E. E. A. Van der Akker (2012). Direct numerical simulation of the turbulent flow in a baffled tank driven by a Rushton turbine, *AIChE Journal* 58, 3878-3890.

Heim, A. and J. Stelmach (2011). The comparison of velocities at the self-aspirating disk impeller level, *Przemysł Chemiczny* 90(9), 1642-1646. (in Polish)

Joshi, B. J., N. K. Nere, C. V. Rane, B. N. Murthy, C. S. Mathpati, A. W. Patwardhan and V. V. Ranade (2011a). CFD simulation of stirred tanks: Comparison of turbulence models. Part I: Radial flow impellers, *The Canadian Journal of Chemical Engineering* 89, 23-82.

Joshi, B. J., N. K. Nere, C. V. Rane, B. N. Murthy, C. S. Mathpati, A. W. Patwardhan and V. V. Ranade (2011b). CFD simulation of stirred tanks: Comparison of turbulence models. (Part II: Axial flow impellers, multiple impellers and multiphase dispersions), *The Canadian Journal of Chemical Engineering* 89, 754-816.

Ju, F., Z. M. Cheng, J. H.Chen, X. H.Chu, Z. M. Zhou and P. Q. Yuan (2009). A novel design for a gas-inducing impeller at the lowest critical speed, *Chemical Engineering Research and Design* 87, 1069-1074.

Kresta, S. M. and P. E. Wood (1993). The flow field produced by a pitched blade turbine: Characterization of the turbulence and estimation of the dissipation rate, *Chemical Engineering Science* 48(10), 1761-1774.

Kuncewicz Cz., F. Rieger, M. Pietrzykowski and J. Stelmach (2013). 3D/2D hybrid model for ribbon impellers operating in laminar regime, *Chemical Engineering and Processing: Process Intensification* 73, 50-58.

Kuncewicz, Cz. and J. Stelmach (2012). Mass transfer coefficients during aeration by self-aspirating impeller, *Proceedings of the 14th European Conference on Mixing*, Warsaw, Poland.

Kuncewicz, Cz. and M. Pietrzykowski (2006). A 3D/2D hybrid model for ribbon impellers operating in laminar motion, *Proceedings of the 12th European Conference on Mixing*, Bologna, Italy.

Kurasiński, T. and Cz. Kuncewicz (2009). Liquid circulation in a mixer and its influence on mass transfer in the gas-liquid system, *Inżynieria i Aparatura Chemiczna* 48(40), 75-76.

Kurasiński, T., J. Stelmach and Cz. Kuncewicz (2004). Liquid velocities in a stirred tank. Data analysis. *Inżynieria i Aparatura Chemiczna*, 3s, 43(35), 89-90.

La Fontaine, R. F. and I. C. Shepherd (1996). Particle image velocimetry applied to a stirred vessel, *Experimental Thermal and Fluid Science* 12, 256-264.

Lee, K. C. and M. Yianneskis (1998). Turbulence properties of the impeller stream of Rushton turbine, AIChE Journal 44, 13-24.

Murthy, B. N., N. A. Deshmukh, A. W. Patwardhan and J. B. Joshi (2007). Hollow felf-inducing impellers: Flow visualization and CFD simulation, *Chemical Engineering Science* 62,

3839-3848.

Murthy, B. N., R. B. Kasundra and J.B. Joshi (2008). Hollow self-inducing impellers for gas-liquid-solid dispersion: Experimental and computational study, *Chemical Engineering Journal* 141, 332-345.

Myers, K. J., R. W. Ward and a. Bakker (1997). A digital particle image velocimetry investigation of flow field instabilities of axial-flow impellers, *Journal of Fluids Engineering* 119, 623-632.

Patwardhan, A. W. and J. B. Joshi (1999). Design of gas-inducing reactors, *Journal of Industrial and Engineering Chemistry* 38, 49-80.

Poncin, S., C. Nguyen, N. Midoux and J. Breysse (2002). Hydrodynamics and volumetric gas-liquid mass transfer coefficient of a stirred vessel equipped with gas-indicing impeller, *Chemical Engineering Science* 75, 3299-3306.

Rzyski, E. and J. Stelmach (2002). Velocity fluctuations during mixing of non-newtonian liquid, *Inżynieria i Aparatura Chemiczna* 4s, 41(33), 113-115.

Saravavan, K. and J. B. Joshi (1995). Gas-inducing-type mechanically agitated contactors: Hydrodynamic Characteristics of multiple impellers, *Journal of Industrial and Engineering Chemistry* 34, 2499-2514.

Saravavan, K., V. D. Mundale and J. B. Joshi (1995). Gas inducing type mechanically agitated contactors, *Journal of Industrial and Engineering Chemistry* 33, 2226-2241.

Sharp, K. V. and R. J. Adrian (2001). PIV study of small-scale flow structure around a Rushton turbine, *Fluid mechanics and Transport Phenomena* 47, 766-777.

Stelmach, J, E. Rzyski and A. Heim (2002). Mean velocity distribution at the self-aspirating disk impeller level, *Inżynieria i Aparatura Chemiczna* 4s, 41(33), 115-115.

Stelmach, J. (2014). *Hydrodynamics of two-phase liquid-gas system. Use of photooptics methods*. Lodz University of Technology, Lodz, Poland.

Stelmach, J., E. Rzyski and F. Rieger (2003b). Energy spectrum of eddies in the tank with a self-aspirating disk impeller, *Inżynieria i Aparatura Chemiczna* 3s, 42(34), 145-147.

Stelmach, J., E. Rzyski and A. Kania (2003a). Energy dissipation on the level of a self-aspirating disk impeller, *Proceedings of the 11th European Conference on Mixing*, Bamberg, Germany.

Wu, H. and G. K. Patterson (1989). Laser-Doppler measurements of turbulent-flow parameters in a stirred mixer, *Chemical Engineering Science* 44(10), 2207-2221.